IVYSPRING
INTERNATIONAL PUBLISHER

Theranostics

Research Paper

SiRNA Delivery with PEGylated Graphene Oxide Nanosheets for Combined Photothermal and Genetherapy for Pancreatic Cancer

Feng Yin[1]*, Kuan Hu[1]*, Yangzi Chen[1], Mengying Yu[1], Dongyuan Wang[1], Qianqian Wang[1], Ken-Tye Yong[2], Fei Lu[1]✉, Yongye Liang[3]✉ and Zigang Li[1]✉

1. School of Chemical Biology and Biotechnology, Peking University Shenzhen Graduate School, Shenzhen, 518055, China;
2. School of Electrical and Electronic Engineering, Nanyang Technological University, Singapore 639798, Singapore;
3. Department of Materials Science and Engineering, South University of Science and Technology of China, Shenzhen, 518055, China.

* These authors contributed equally to this work.

✉ Corresponding authors: Zigang Li, email: lizg@pkusz.edu.cn; Fei Lu, email: lufei@pkusz.edu.cn; Yongye Liang, email: liangyy@sustc.edu.cn.

Abstract

Since the successful exfoliation of graphene from graphite in 2004, graphene and graphene oxide (GO) have been considered the most promising two-dimensional (2D) nanomaterials with distinguished physical and chemical characteristics and have attracted great attention in many different fields. Graphene oxide is well-known for its distinct physiochemical properties and shows only minimal cytotoxicity compared to carbon nanotubes. Until now, only limited efforts have been invested in utilizing GO for gene therapy in pancreatic cancer treatments. In this study, we utilized multi-functionalized monolayer GO as a gene delivery system to efficiently co-deliver HDAC1 and K-Ras siRNAs (small interfering RNAs targeting the HDAC1 gene and the G12C mutant K-Ras gene, respectively) to specifically target pancreatic cancer cells MIA PaCa-2. The systematic mechanistic elucidation of the dual gene silencing effects indicated the inactivation of both the HDAC1 and the K-Ras gene, thereby causing apoptosis, proliferation inhibition and cell cycle arrest in treated MIA PaCa-2 cells. The synergistic combination of gene silencing and NIR light thermotherapy showed significant anticancer efficacy, inhibiting *in vivo* tumor volume growth by >80%. Furthermore, GO can be metabolized in the mouse model within a reasonable period of time without obvious side effects. Based on preliminary *in vivo* application, this study for the first time indicates the promising potential of functionalized GO as a vehicle for gene therapy delivery with low toxicity for the treatment of pancreatic adenocarcinoma.

Key words: Graphene Oxide (GO), siRNA, HDAC1, K-Ras, Folic acid (FA), Pancreatic cancer.

Introduction

Thanks to their finely tunable particle sizes and multi-functional surfaces, nanomaterials have attracted much attention in biomedical fields [1]. Over the past decades, a vast range of nanomaterials including liposomes [2], silica nanoparticles [3], metal-based nanoparticles [4], carbon nanoparticles [5] and quantum dots [6] have been developed for applications in biomedicine, especially in cancer theranostics. Two-dimensional (2D) nanomaterials with excellent electronic, optical and chemical properties have been identified as novel therapeutic agents for use in biomedicine [7, 8]. Graphene, the best-known 2D nanomaterial, was first discovered in 2004 [9] and has since been extensively tested for applications in electronics and optics [10], catalysis [11], sensors [12], energy storage [13] and biomedical devices [14]. GO is a graphite oxide monolayer obtained by exfoliating graphite oxide into layered

sheets which can then be dispersed in water thanks to abundant hydrophilic surface groups such as hydroxyl and carboxyl groups [15]. These surface groups can easily be functionalized with biocompatible polyethylene glycol (PEG) polymers, which endow GO with high biocompatibility and loading capacity [16]. Furthermore, numerous toxicology studies have indicated that GO coated with a biocompatible material, such as protein or PEG, exhibited negligible in vitro or in vivo toxicity [17, 18]. Therefore, functionalized graphene oxide has been developed into ideal gene delivery systems [19-21]. In addition to being ideally suited for drug delivery, GO exhibits superior optical absorption and strong optical near-infrared (NIR) conversion properties. These photo-thermal effects could be useful in biomedical applications, including cancer therapy [22, 23]. However, there are few reports on the biomedical applications of GO *in vivo*, especially in the context of cancer treatment [24-26].

Since the first successful nuclear gene transfer in humans in 1989 [27], gene therapy has been extensively studied as a means of treating various diseases, such as cardiovascular diseases [28], diabetes [29], immunodeficiency diseases [30] and cancers [31]. RNA interference (RNAi), the most broadly utilized form of gene therapy, works in a dose-dependent manner with high gene knockdown efficiency [32, 33]. The main limitations of RNAii include low *in vivo* uptake efficiency and the natural instability of RNA. Therefore, numerous nanomaterials have been functionalized and developed into siRNA delivery systems for biomedical applications [4, 34, 35]. In this study, two genes, Histone deacetylase 1 (HDAC1) and K-Ras, with essential roles in the growth of pancreatic cancer cells but no obvious effects in normal cells, were chosen for siRNA-mediated knockdown. HDAC1 plays a unique role in maintaining the pluripotency of embryonic and cancer stem cells [7, 36] and is highly expressed in pancreatic adenocarcinoma and other malignant tumors [37] where it regulates cell transformation, survival, invasion and metastasis [38-40]. K-Ras mutations are observed in over 90% of pancreatic cancers and could represent a potential target for pancreatic cancer therapy [41]. To overcome the natural instability [42] and low uptake efficiency of siRNA in vivo [43], we utilized multifunctional GO as the gene delivery system to target pancreatic cancer cells.

We have previously shown that the co-delivery of siRNA and the anticancer drug doxorubicin using gold nanorods (AuNRs) as nanocarriers exhibited superior efficacy in the *in vitro* and *in vivo* treatment of pancreatic cancer, suggesting synergistic effects of chemotherapy, RNA silencing and photothermal therapy [4]. Here, we developed a novel gene delivery system utilizing functionalized GO nanoparticles by conjugating folic acid (FA), NH_2-mPEG-NH_2 (5k) and Poly-allylamine hydrochloride (PAH) onto GO nanosheets and tested their application in pancreatic cancer therapy by co-delivering HDAC1 and K-Ras siRNAs (directed against a G12C mutant K-Ras gene, special mutant siRNA for MIA PaCa-2cells [44]) *in vitro* and *in vivo* (Fig.1). Folate Receptor-expressing (FR+) cancer cells, such as the pancreatic cancer cell line MIA PaCa-2 and the breast cancer cell line MCF7, can take up conjugates of folic acid with GO via receptor-mediated endocytosis, thus allowing for the targeted delivery of cargo [45, 46]. The co-delivery of HDAC1 and K-Ras siRNA by PAH/FA/PEGylated GO nanosheets resulted in high rates of internalization in MIA PaCa-2 cells and inhibited cell proliferation by >80%. Furthermore, synergistic effects between gene therapy and photothermal activity exhibited by these GO nanosheets under NIR light inhibited the *in vivo* tumor growth rate by over 80%. *In vivo* imaging studies demonstrated that the functionalized GO/siRNA nanocomplexes preferentially accumulated in tumor sites. Importantly, treatment with PAH/FA/PEGylated GO nanocomplexes did not affect the body weight, learning ability, memory management or voluntary movement of mice compared to untreated control mice, and histological analyses did not identify side effects in the major organs of treated mice. Therefore, this study is the first to demonstrate the promising potential of GO nanosheets as a gene delivery system and to develop a novel, relatively non-toxic nanoplatform combining targeted gene therapy and photothermal effects for the treatment of pancreatic cancer.

Materials and methods

Synthesis of NH_2/PEG/FA polymers

First, the amine-functionalized Boc-NHmPEG-NH_2 was conjugated with activated FA to prepare an FA-conjugated, Boc-protected, bifunctional 5k FA-NH-mPEG-NH-Boc polymer. 100 mg of FA was briefly mixed with 50 mg DCC (N, N'-dicyclohexylcarbodiimide) and 35 mg NHS (N-Hydroxysuccinimide) in 3 mL anhydrous DMSO at room temperature (RT). After 15 minutes, 500 mg NH_2-mPEG-NH-Boc in 5 mL DMSO was added and allowed to react at RT for 24 hours with stirring before PEG was precipitated from the mixture solution with 50 mL cold diethyl ether. The product was washed 3 times with 5 mL diethyl ether and dried under vacuum. The yellowish product was then dissolved in

water, filtered to remove any insoluble remnants and confirmed by MALDI-TOF and NMR (Fig. S2).

Preparation of PEG- or FA/PEG-coated GO nanosheets

To deprotect the Boc group, 2 mL TFA were added to 100 mg FA-mPEG-NH-Boc dissolved in dichloromethane and incubated while stirring for 3 hours at RT. After evaporating the TFA solvent, the remaining solid was dissolved in 10 mL water. The final product, NH$_2$-mPEG-FA, was lyophilized and stored at -20°C.

For GO functionalization, we modified a previously published protocol [47]. Briefly, 1 mg of GO (0.5 mg/mL, ultrapure DI water) was mixed with 10 mg of mPEG/NH$_2$ or FA/PEG/NH$_2$. The resulting PEGylated or FA/PEGylated GO nanosheet mixtures were sonicated for 30 minutes. Afterwards, 10 mg EDC (3-(ethyliminomethyleneamino)-N,N-dimethyl-propan-1-amine) was added, and the mixture was stirred vigorously for 24 hours. Excess unbound mPEG/NH$_2$ or FA/PEG/NH$_2$ polymers were removed by two rounds of centrifugation (10000 rpm, 25-30 minutes). The precipitate was resuspended in 1 mL of ultrapure water and sonicated again. A final PEGylated GO nanosheet concentration of 1 mg/mL was obtained.

For siRNA loading, PAH was pre-dissolved in ultrapure deionized (DI) water. PEGylated GO nanosheets (1 mg/mL) were mixed with PAH (10 mg/mL) in 2 mL ultrapure DI water at a volume ratio of 1:1. The mixture was stirred for 36 hours at RT. Free PAH was removed by centrifugation.
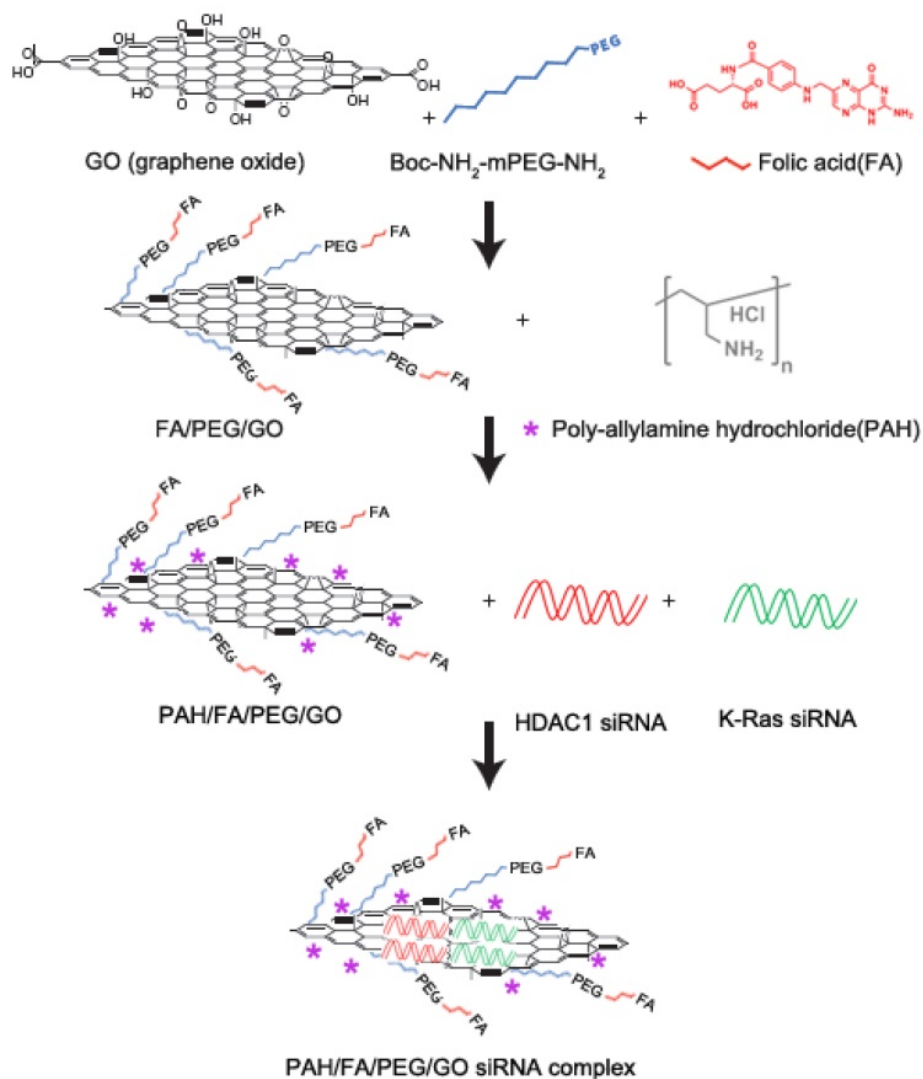

Figure 1. Schematic overview of the FA/PEG/GO synthesis and gene loading process using engineered GO-based nanocarriers. Folic acid (FA) was conjugated with NH$_2$-mPEG-NH$_2$ to form FA/PEG-NH$_2$. Subsequently, FA/GO nanosheets were prepared by conjugating the amine-functionalized FA/PEG-NH$_2$ to increase water solubility and biocompatibility. For siRNA delivery, PEGylated or FA/PEGylated GO were functionalized with positive polymer PAH to form positively charged GO/PEG/PAH or GO/PEG/FA/PAH which were able to deliver siRNA by electrostatic interaction.

GO and PEGylated GO characterizations

SEM images were obtained using a JEOL-5600LV scanning electron microscope at an acceleration voltage of 5 kV. GO samples were deposited onto a quartz substrate and sputter-coated to a projected thickness of ~5 nm. Transmission electron microscopy (TEM) images were obtained using a JEOL model JEM-2010 transmission electron microscope at an acceleration voltage of 200 kV. The specimens were prepared by drop-casting the sample dispersion onto a carbon coated 300 mesh copper grid (Carbon Type-B, Ted Pella, Inc.). After coating the samples on the grid, uranyl acetate solution (2%, 10 mL) was added dropwise onto the grid for negative staining. The UV absorption spectra were determined using a Shimadzu UV-2450 spectrophotometer. The hydrodynamic size distribution profiles and the zeta potentials of the GO or PEGylated GO nanocomplexes were measured using a particle size analyzer system (90 Plus, Brookhaven Instruments).

AFM (atomic force microscopy) measurements were obtained using a Nanoscope V multimode atomic force microscope (Veeco Instruments, USA). Samples for AFM images were diluted with deionized water to yield a final concentration of 1×10^{-6} M. The sample (20 μL) was then dispersed on freshly cleaved muscovite mica and allowed to dry at RT. Images were acquired using tapping mode under ambient conditions.

Raman spectra were determined on a Renishaw InVia Reflex Raman system (Renishawplc, Wotton-under-Edge, UK) using a grating spectrometer with a Peltier-cooled charge-coupled device (CCD) detector coupled to a confocal microscope. The spectra were then processed with Renishaw WiRE 3.2 software. Raman scattering was excited using an argon ion laser (I = 514.5 nm). The D-mode is caused by the disordered structure of graphene. The presence of disorder in sp2-hybridized carbon systems results in resonance Raman spectra, and thus makes Raman spectroscopy one of the most sensitive techniques to characterize disorder in sp2 carbon materials. The G-mode is at about 1583 cm-1 and is due to E2g mode at the Γ-point. G-band arises from the stretching of the C-C bond in graphitic materials and is common to all sp2 carbon systems.

In vivo dual gene and photothermal therapy using PEGylated-GO nanocarriers

Athymic nude mice (BALB/cASlac-nu) were obtained from Vital River Laboratory Animal Technology Co. Ltd. of Beijing, People's Republic of China and allowed an acclimation period of 1 week. Mice were maintained in an isolated biosafety facility for specific pathogen free (SPF) animals with sterile bedding, food and water. All operations were carried out in accordance with the National Standard of Animal Care and followed accepted procedures at Shenzhen Institutes of Advanced Technology, Chinese Academy of Science, Guangdong Province, People's Republic of China (permit number SIAT-ITB-160128-YYS-LZG-A0164).

For tumor suppression assays, athymic nude mice (female; 6 weeks old) were inoculated subcutaneously in the lower flank with 1×10^7 *in vitro*-propagated MIA PaCa-2 cells that were trypsinized, harvested and resuspended in 100 μL DMEM. After 10-15 days, mice with tumors exceeding 100-150 mm^3 in volume were randomly divided into 5 groups of 8-9 mice. 3-4 mice per treatment group were sacrificed after 21 days for tumor inhibition imaging while the others were maintained for survival curves. Mice bearing MIA PaCa-2 tumors were treated with different FA/PEGylated GO nanoformulations by intraperitoneal injection as follows: group 1, no treatment (PBS); group 2, FA/GO+NIR light (4 mg/kg, injection); group 3, FA/GO/scramble siRNA(FA/GO 4 mg/kg, siRNA 32 μg (1 nmol, injection); group 4, FA/GO/ (HDAC1+Kras) siRNA [FA/GO 4 mg/kg, siRNA 16 μg per gene for each mouse, injection]; group 5, FA/GO/ (HDAC1+Kras) siRNA [FA/GO 4 mg/kg, siRNA 16 μg per gene for each mouse, injection] with 808 nm NIR light (1W) for 1 min after injection. Mice were injected once every 4 days starting on day 0. Tumor volumes were measured using calipers (accuracy of 0.02 mm) every other day and calculated using the following formula: V= L×W^2/2 (W, the shortest dimension; L, the longest dimension). Each tumor was independently measured, and fold-changes in volume were calculated relative to the volume on day 0. Statistical significance between groups was determined by one-way analysis of variance (ANOVA).

Results

Schematic illustration and characterization of multifunctional GO-based siRNA delivery systems

Graphene oxide (GO) is an important graphene derivative functionalized with oxygen-containing chemical groups that can be obtained by exfoliating graphite oxide into layered sheets through sonication or mechanical stirring [48]. In our system, there were 5 types of GO-based nanoformulation as follows (Fig. 1 and Table S1): (i) naked GO nanosheets functionalized with PEG (GO/PEG); (ii) GO/PEG formulation modified with PAH polymer (GO/PEG/PAH); (iii) GO/FA/PEG formulation modified with PAH polymer (GO/FA/PEG/PAH);

(iv) siRNA molecules delivered by GO/PEG/PAH (GO/siRNA); (v) siRNA molecules delivered by GO/FA/PEG/PAH (FA/GO/siRNA).

Monolayer 2D GO nanosheets were synthesized as previously described [49] and confirmed via scanning electron microscopy (SEM) and transmission electron microscopy (TEM) (Fig. 2A and Fig. S1). To increase water solubility and biocompatibility, we developed functionalized GO nanosheets with PEG (GO/PEG) or folic acid (FA)-modified PEG (GO/PEG/FA). For siRNA delivery, PEGylated or FA/PEGylated GO were functionalized with PAH polymer to form GO/PEG/PAH or GO/PEG/FA/PAH, respectively. After PEGylation, the average diameter of PEGylated GO decreased to about 400 nm and exhibited high solubility and stability (Fig. 2B). This decrease in size was also verified by dynamic light scattering (DLS) measurements (Fig. S1). As shown in Raman intensities, the ratio of the D to G bands (I_D/I_G) of GO and GO/PEG were 1.037 and 0.9848, respectively [50] (Fig. 2C). The absorbance spectra of different GO nanocomplexes retained the same optical absorption peak at 230 nm, indicating that the properties of GO

were not affected by the surface PEG modification. The successful conjugation was further confirmed by the presence of a strong optical absorption peak at 280 nm [51] (Fig. 2D). With different materials functionalized on the surface of GO, the hydrodynamic diameters (Table S1) and zeta potentials changed significantly (Fig. 2E). The zeta potential of bare GO was measured at -55.68 mV. The incubation with PAH added strong positive charges for siRNA delivery to GO nanocomplexes. Furthermore, the zeta potential of the nanocomplexes was dependent on the incubation ratio between GO/PEG/PAH (GO) or GO/FA/PEG/PAH (FA/GO) and siRNA (Fig. S3). The total amount of positively charged GO or FA/GO nanosheets necessary to completely bind a given amount of siRNA molecules were determined by gel retardation assays. The total amount of free siRNA molecules decreased drastically with increasing addition of GO or FA/GO nanosheets (Fig. S3). Based on the gel retardation results, the optimal mass ratio between FA/GO and siRNA molecules was 1 µg: 1 µg, which was used for all *in vitro* and *in vivo* experiments.
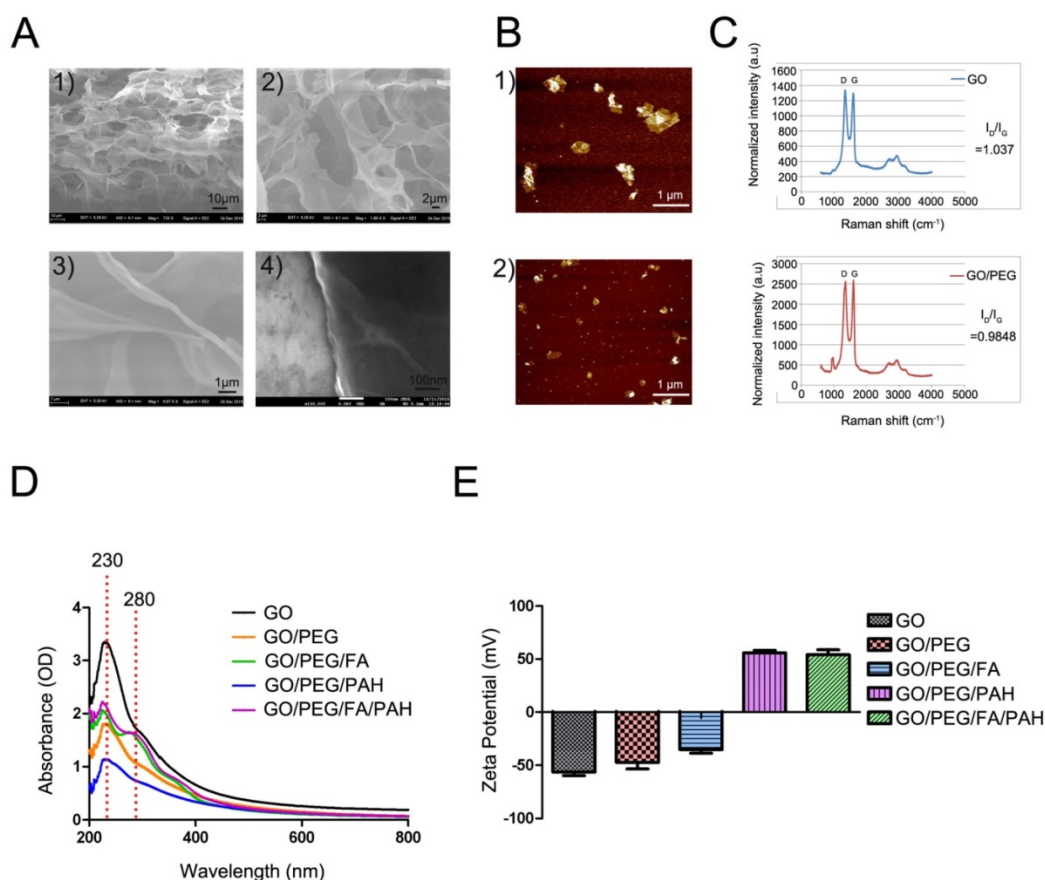

Figure 2. Characterization of the engineered GO-based nanocarriers. (A) Scanning electron microscope images of monolayer 2D GO nanosheets. (B) AFM images of GO before 1) and after 2) PEGylation. (C) Raman spectra of GO and PEGylated GO. The intensity ratios (I_D/I_G) of GO and PEGylated GO were about 1.037 and 0.9848, indicating the reduction of GO after the removal of oxygen moieties by PEG/NH$_2$. (D) Absorption spectra of different GO-based nanocarriers. (E) Surface zeta potential of different GO nanoformulations. All experiments were performed in duplicates with consistent results. Values are expressed as means ± SEM, n = 3.

Efficient co-delivery of HDAC1 and K-Ras siRNAs by FA/GO nanoformulations into MIA PaCa-2 cells

According to previous studies, HDAC1 plays an essential role in maintaining the pluripotency of embryonic and cancer stem cells [7]. Furthermore, HDAC1 is overexpressed in many malignant tumors, including pancreatic, colorectal and lung cancer, where it regulates cell transformation, survival, invasion and metastasis [37, 52]. In our study, we utilized PEGylated GO nanosheets as the gene delivery system to co-deliver HDAC1 and K-Ras siRNAs (the G12C mutant K-Ras gene, special mutant siRNA for MIA PaCa-2 cells) into MIA PaCa-2 cancer cells. The cellular uptake efficiency and intracellular distribution of HDAC1 siRNA^{FAM} and K-Ras siRNA^{Cy3} were monitored using fluorescence microscopy (Fig. 3). The MIA PaCa-2 cells were treated with various GO nanoformulations for 4 hours before examination by fluorescence microscopy. The strongest red (Cy3) and green (FM) fluorescent signals in cells demonstrated that both siRNAs were successfully co-delivered into MIA PaCa-2 cells by FA/GO nanosheets (Fig. 3). As a comparison, weaker fluorescence signals were observed from MIA PaCa-2 cells treated with FA-unconjugated GO nanoformulations (Fig. 3D). As expected, no fluorescence signals were observed from cells treated with PBS, FA/GO/PAH or free HDAC1 siRNA^{FAM} and K-Ras siRNA^{Cy3} (Fig. 3 A-C), which suggested that the siRNA molecules alone were incapable of penetrating the cell membrane due to their negatively-charged nature and rapid degradation in biological fluid environments. It is worth noting that the fluorescence signals from cells treated with the commercially available transfection reagents Lipofectamine 2000 and Oligofectamine were much weaker than those of cells treated with siRNA and FA/GO nanocomplexes (Fig. 3 F and G).
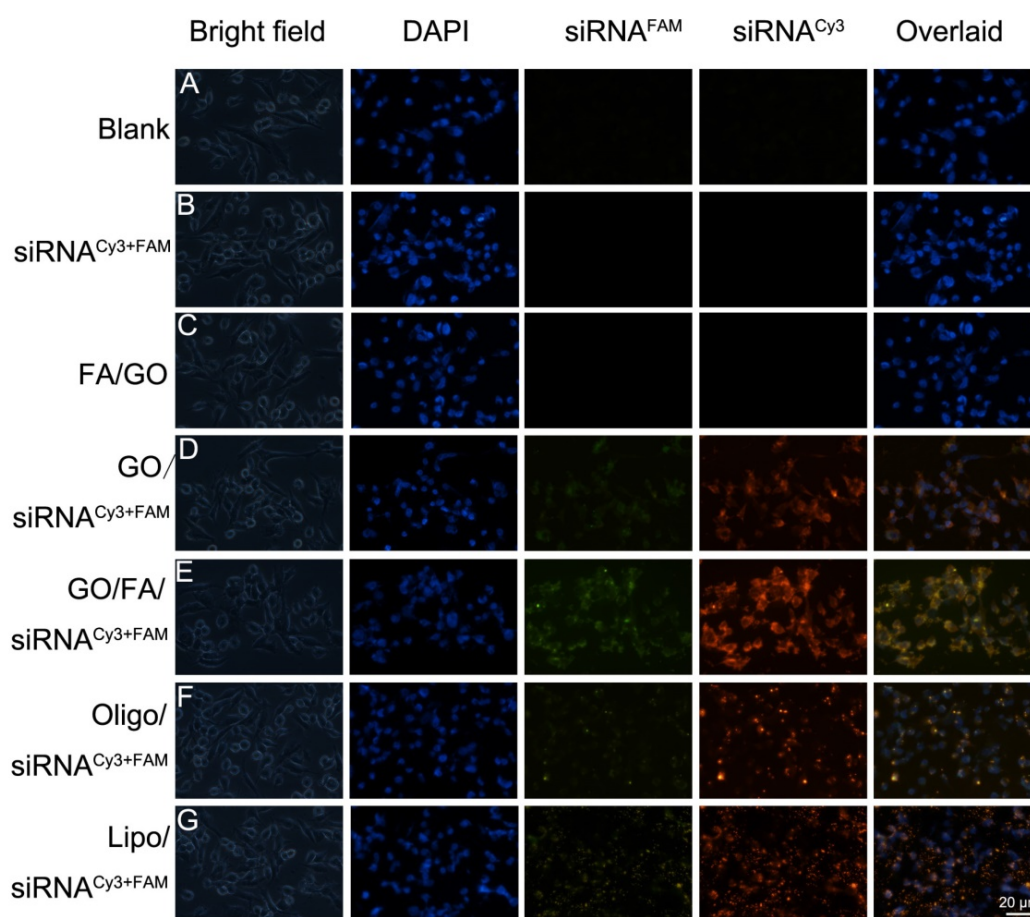

Figure 3. Fluorescent images of MIA PaCa-2 cells after incubation with different GO/siRNA nanoformulations for 4 hours. (A) PBS only (blank); (B) free K-Ras siRNA^{Cy3} + HDAC1 siRNA^{FAM} (abbreviated as siRNA$^{FAM+Cy3}$) and (C) FA/PEG/PAH/GO (FA/GO) (negative controls); (F) Oligofectamine-conjugated siRNA (Oligo/siRNA$^{FAM+Cy3}$) and (G) Lipofectamine 2000 (Lipo/siRNA$^{FAM+Cy3}$) (positive controls); and Kras-siRNA^{Cy3} and HDAC1-siRNA^{FAM} co-delivery by (D) GO/PEG/PAH (abbreviated as GO/siRNA$^{FAM+Cy3}$) or (E) GO/PEG/PAH/FA (abbreviated as GO/FA/siRNA$^{FAM+Cy3}$). The cell nuclei were stained with DAPI (pseudo-colored in blue), and signals from FAM and Cy3 were designated in green and red, respectively. Bright field images were merged with DAPI and siRNA$^{FAM+Cy3}$ (overlaid) to indicate the cell-penetrating abilities of different complexes.

These results demonstrated that the use of FA/GO nanoformulations could efficiently deliver siRNAs into cells and protect siRNA from degradation (Fig. S3 D), suggesting that they may represent a promising alternative to commercial transfection reagents for gene delivery.

Flow cytometry analysis was performed to further quantitate the delivery efficiency of HDAC1 siRNA[FAM] and K-Ras siRNA[Cy3] by GO nanoformulations (Fig. 4 and Fig. S4). Figure 4A shows the fluorescence plots of MIA PaCa-2 cells treated with different GO nanoformulations. Cells treated with PBS, FA/GO or free HDAC1 siRNA[FAM] and K-Ras siRNA[Cy3] were used as negative controls. Figures 4B and 4C show the corresponding transfection efficiencies and average fluorescence signals, respectively. MIA PaCa-2 cells treated with FA/GO/(H+K) siRNA[Cy3+FAM] nanoformulations exhibited the strongest FAM and Cy3 fluorescence signals, and their corresponding transfection efficiencies were estimated at 90% and 95%, respectively. Their fluorescence signals were much higher than those of cells treated with GO/siRNA[Cy3+FAM] nanoformulations (transfection efficiencies of 60% and 65%, respectively) or Oligofectamine/siRNA nanoformulations (transfection efficiencies of 61% and 78%, respectively). Other FR+ cancer cells (such as Panc-1 and HeLa cells) also exhibited the strongest uptake of FA/GO/siRNA (Figure S4). HepG2 cells (FR- cancer cells) and Raw264.7 cells showed indistinguishable uptake efficiencies of GO/siRNA and FA/GO/siRNA. Furthermore, FA pre-treatment of MIA Paca-2 cells blocked surface FRs and prevented the enhancement of fluorescence signals in cells treated with FA/GO/siRNA nanoformulations. These differences demonstrated the successful enhancement of cellular uptake of GO nanoformulations by the conjugation of FA. As negative controls, cells treated with PBS, FA, FA/GO or free HDAC1 siRNA[FAM] and free K-Ras siRNA[Cy3] showed almost no fluorescence signals. These results are consistent with those from the cell fluorescence imaging analyses in Figure 3.
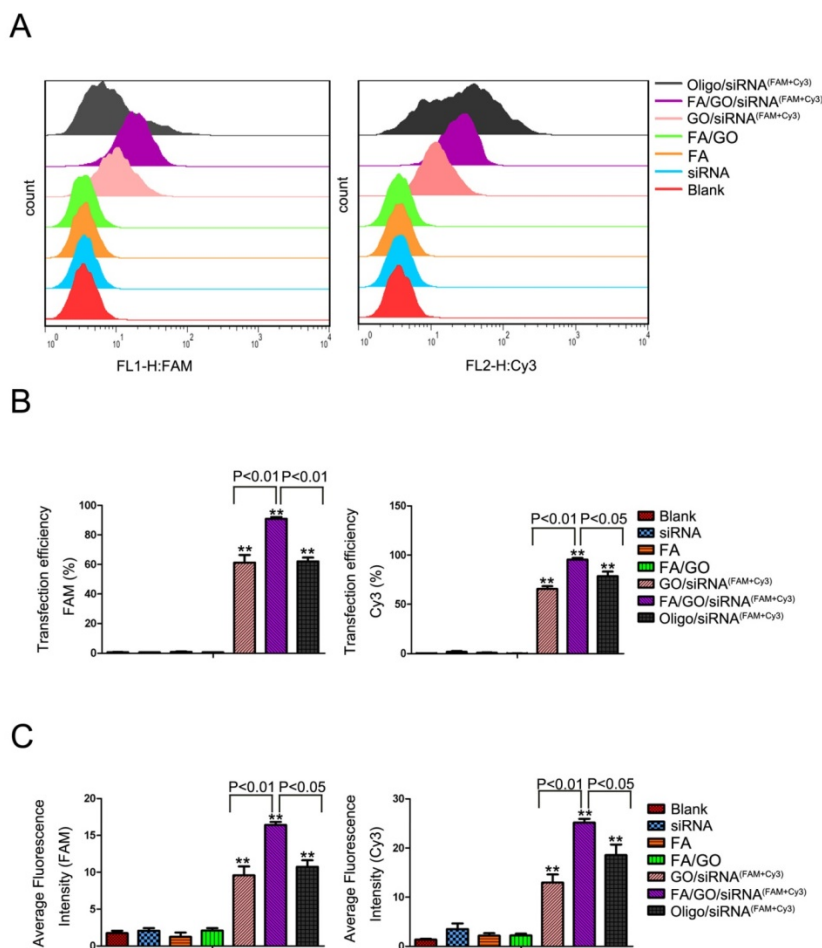

Figure 4. Flow cytometry evaluations of the transfection efficiencies of MIA PaCa-2 cells treated with different nanoformulations. (A) Statistical cell counts by flow cytometry, where the y-axis represents cell counts and the x-axis the FAM and Cy3 fluorescence intensities, respectively. (B) Transfection efficiency and (C) average fluorescence intensity from experiments shown in (A). Values are expressed as means ± SEM, n = 3; **, P < 0.01 vs Control, GO/FA, siRNA[FAM] and siRNA[Cy3].

GO-based siRNA delivery system efficiently co-delivers siRNAs into cells and induces target gene knockdown in pancreatic cancer cells

Given the critical roles of HDAC1 and mutant K-Ras in pancreatic cancer, specific siRNAs targeting these genes were delivered into MIA PaCa-2 cells by GO nanoformulations for pancreatic cancer gene therapy. The amount of gene knockdown of HDAC1 and K-Ras was confirmed at both the mRNA and the protein level in MIA PaCa-2 cells treated with FA/GO/siRNA nanoformulations (Fig. 5). Compared to PBS-treated cells (blank control), cells treated with FA/GO or FA/GO/scramble siRNA exhibited no obvious changes in the mRNA or protein levels of HDAC1 and K-Ras.
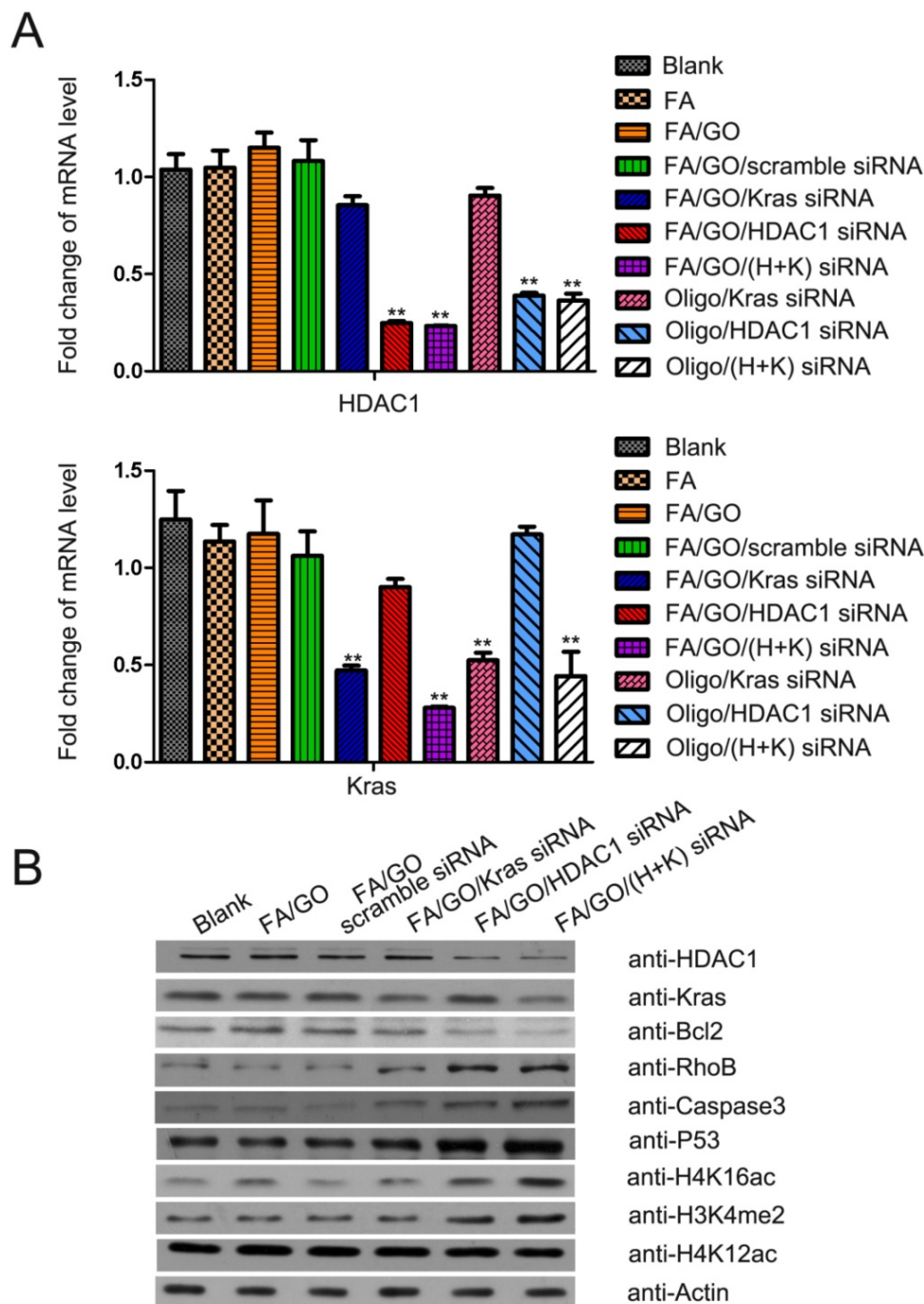

Figure 5. Target gene expression in MIA PaCa-2 cells treated with different nanoformulations. MIA PaCa-2 cells were treated with PBS, FA, FA/GO, FA/GO/scramble siRNA, FA/GO/K-Ras siRNA, FA/GO/HDAC1 siRNA, FA/GO/(H+K) siRNA, Oligo/K-Ras siRNA, Oligo/HDAC1 siRNA and Oligo/(H+K) siRNA for 4 hours. All cells were then washed with PBS and re-incubated in fresh cell media for an additional 44 hours. (**A**) Relative mRNA levels as detected by RT-PCR. (**B**) Relative protein levels as detected by western blotting. Actin was used as the protein loading control. Data are presented as means ± SEM of triplicate experiments. **, $P < 0.01$ vs PBS (blank).

On the other hand, cells treated with FA/GO/HDAC1 siRNA, FA/GO/K-Ras siRNA or FA/GO/(HDAC1+K-Ras) siRNAs showed remarkable inhibition of HDAC1 and K-Ras gene expression. Furthermore, mRNA levels of HDAC1 or K-Ras in cells treated with Oligofectamine/siRNA were higher than in cells treated with FA/GO/siRNA nanoformulations, which was consistent with cell fluorescent imaging and flow cytometry results. Since HDAC1 inactivation changes histone methylation and acetylation patterns [7, 36], we investigated the modification levels of acetylated H4K16, acetylated H4K12 and methylated H3K4 (Fig. 5B). Western blot analyses showed that the loss of HDAC1 in cells treated with FA/GO/siRNA nanoformulations caused notable accumulation of dimethylated H3K4 and acetylated H4K16. These results confirm the great potential of GO-based nanoformulations as effective siRNA delivery systems to knock down target genes for gene therapy in cancer and other diseases.

The downregulation of HDAC1 and K-Ras by FA/GO/siRNA nanoformulations causes growth inhibition, apoptosis and cell cycle arrest of MIA PaCa-2 cells

Based on the gene knockdown results in Figure 5, HDAC1 siRNA and K-Ras siRNA delivered by FA/GO nanoformulations could efficiently suppress the expression of HDAC1 and K-Ras, respectively. We further examined the growth inhibition of the cells treated with FA/GO nanoformulations (Fig. 6 and Fig. S4). Compared with PBS-treated cells (blank control), negligible inhibition of cell growth was observed in cells treated with FA/GO or FA/GO/scramble siRNA for 48 and 72 hours. On the other hand, obvious inhibition was observed in cells incubated with FA/GO/HDAC1 siRNA (48.43±2.57% and 45.49±3.17%), FA/GO/K-Ras siRNA (51.17±3.16% and 47.65±0.87%) or FA/GO/HDAC1+K-Ras siRNA (37.92±2.11% and 33.43±1.95%). To assess the toxicity of naked GO or FA/GO, MIA PaCa-2 cells were treated with different concentrations of GO or FA/GO ranging from 0 μg/mL to 100 μg/mL for 48 hours (Fig. S4). Cell viability remained at around 80% even with the highest concentration (100 μg/mL), which clearly demonstrated the high biocompatibility and low toxicity of PEGylated GO-based nanocarriers. The human normal liver cell line QSG7701 was treated with different FA/GO/siRNA nanoformulations to estimate their specificities and toxicities (Fig. S5). The treatment of FA/GO/siRNA nanoformulations led to no obvious growth inhibition of QSG7701 cells.

Therefore, the combination of nanotechnology and gene therapy in our studies may be a promising candidate for pancreatic cancer treatment.

To study the collective effect of HDAC1 and K-Ras on cell apoptosis and cell cycle arrest, MIA PaCa-2 cells were treated with different GO nanoformulations and then evaluated via fluorescence activated cell sorting (FACS) analysis. Figure 7 shows the flow cytometric data of apoptotic cells stained with Annexin V/PI. The pro-apoptotic effect of FA/GO/(HDAC1+K-Ras) siRNA was more pronounced in MIA PaCa-2 cells than that of FA/GO/HDAC1 siRNA or FA/GO/K-Ras siRNA, which is consistent with the viability results. Moreover, the combined inactivation of HDAC1 and K-Ras caused a profound S phase arrest in MIA PaCa-2 cells, with a higher percentage of cells in S phase (27.88%) than with any of the other treatments (Fig. 8). These results show that the co-delivery of HDAC1 and K-Ras siRNA by GO nanocarriers was more efficient in blocking the proliferation of MIA PaCa-2 cells through apoptosis and cell cycle arrest in S phase.

Transcriptome analysis of the roles that HDAC1 and K-Ras play in the proliferation of MIA PaCa-2 cells

To attain an overview of the genes directly affected by the combined inactivation of HDAC1 and K-Ras, genome-wide mRNA microarrays were performed using MIA PaCa-2 cells treated with FA/GO/siRNA nanoformulations (Fig. 9 and Fig. S6). Compared to untreated cells, a total of 1344 downregulated and 766 upregulated genes were detected (fold change >2) and clustered in MIA PaCa-2 cells with inactivation of HDAC1 and K-Ras, which affected more genes than the inactivation of either HDAC1 or K-Ras alone (Fig. 9A and B and Fig. S6). Despite these findings, gene ontology analysis revealed that a number of genes with changed expression levels are involved in different pathways and play important roles in regulating the activity of pancreatic cancer cells, including the P53 signaling pathway, the Ras signaling pathway, and cell cycle and cancer pathways (Fig. 9C and Fig. S6). Several downstream genes were selected as candidates and were confirmed by RT-PCR (Fig. 9D) and western blot (Fig. 5B). Together, these results demonstrate that both HDAC1 and K-Ras serve as key regulators in mediating the activity of pancreatic cancer cells and can therefore be considered promising targets for cancer therapies.
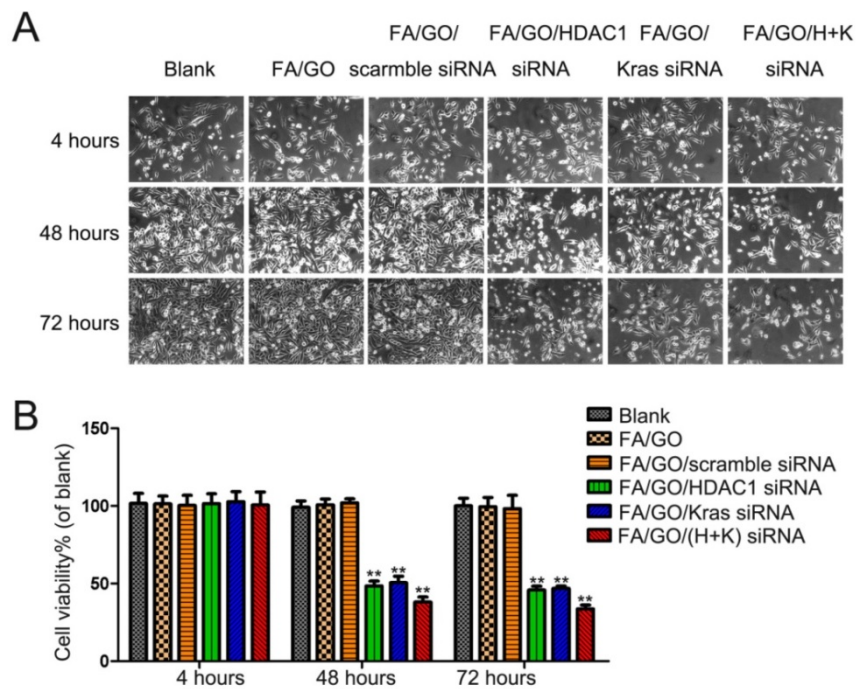
Figure 6. Cell viability tests of different GO-based formulations. The growth of MIA PaCa-2 cells was inhibited by FA/GO/siRNA nanoformulations. Phase contrast microscope images (A) and relative cell viabilities (B) of MIA PaCa-2 cells treated with PBS, FA/GO, FA/GO/scramble siRNA, FA/GO/K-Ras siRNA, FA/GO/HDAC1 siRNA or FA/GO/(H+K) siRNA for 4 hours, washed with PBS and re-incubated in fresh cell media for the designated period of time. Data are presented as means ± SEM of triplicate experiments. *, P < 0.05, **, P < 0.01 vs PBS (blank) and FA/GO.
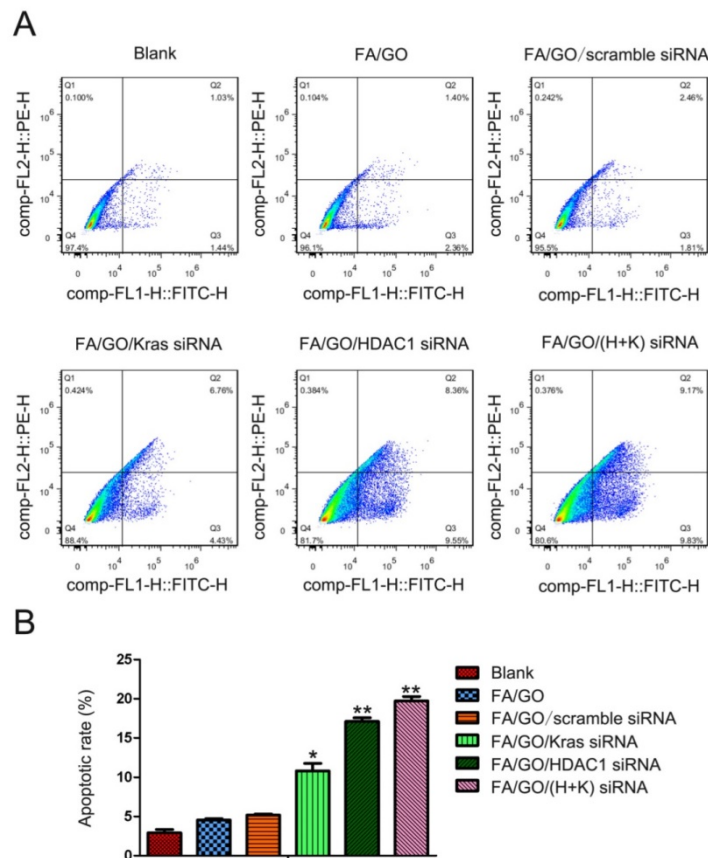

Figure 7. FITC-Annexin V and propidium iodide (PI) cell death assay of MIA PaCa-2 cells 48 hours after treatment with different nanoformulations. (A) The number of apoptotic cells stained with Annexin V/PI was measured by flow cytometry. (B) Late apoptotic cell counts in the upper right quadrant (Q2) and lower right quadrant (Q3) for different treatment groups. Data are presented as means ± SEM of triplicate experiments. *, P < 0.05, **, P < 0.01 vs PBS (blank) and FA/GO.
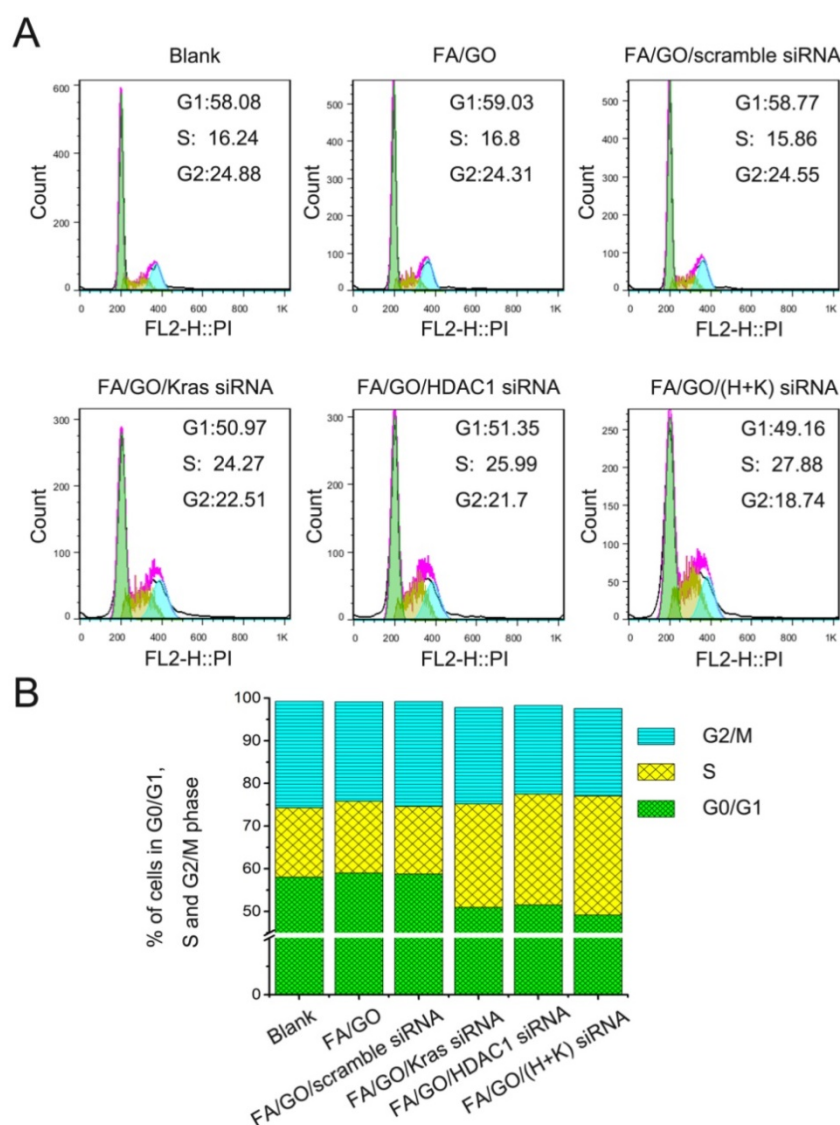
Figure 8. Cell cycle analysis of MIA PaCa-2 cells treated with different nanoformulations. (A) Representative images of flow cytometry analysis 48 hours after treatment. (B) Percentage of MIA PaCa-2 cells in each mitotic phase after treatment with various nanoformulations. A higher proportion of MIA PaCa-2 cells were in S Phase after treatment with HDAC1 and K-Ras siRNA by FA/GO-based nanocarriers than with any other treatment.

GO-based nanoformulations show superior antitumor activities in a MIA PaCa-2 xenograft animal model

To assess whether GO-based nanoformulations would be able to specifically target tumors and suppress tumor growth *in vivo*, we utilized different GO nanoformulations to treat tumor-bearing mice (Fig. 10 and Fig. S7). For special target-imaging, PBS or FA/GO/siRNA[Cy3] nanoformulations were injected into mice by peritoneal or tail vein injection (data not shown), and mice were imaged at different time points (0 hour, 0.5 hour, 2 hours and 4 hours) using the IVIS Lumina II small animal *in vivo* optical imaging system (Fig. S7). The optical signal intensity of FA/GO/ siRNA[Cy3] nanoformulations increased in tumors from 0 to 4 hours, indicating the specific targeting properties for imaging in the near-infrared-emission range. Furthermore, the *ex vivo* fluorescence from tumors and major organs 24 hours after injection was consistent with previous reports [53, 54] on the biodistribution of GO nanoparticles and indicated that the majority of the nanoparticles were accumulating in the tumor, liver and kidney (Table S4). Subsequently, we examined the tumor inhibition of GO-based nanoformulations in the tumor-bearing mice (Fig. 10 and Fig. S8). We also combined NIR light with GO nanocomplexes for the tumor inhibition study because the strong absorption of GO in the near infrared region can induce photon-electron interactions to generate heat *in vitro* or *in vivo* (Fig. S9) which is widely used to drive tumor inhibition and treatments of other diseases.
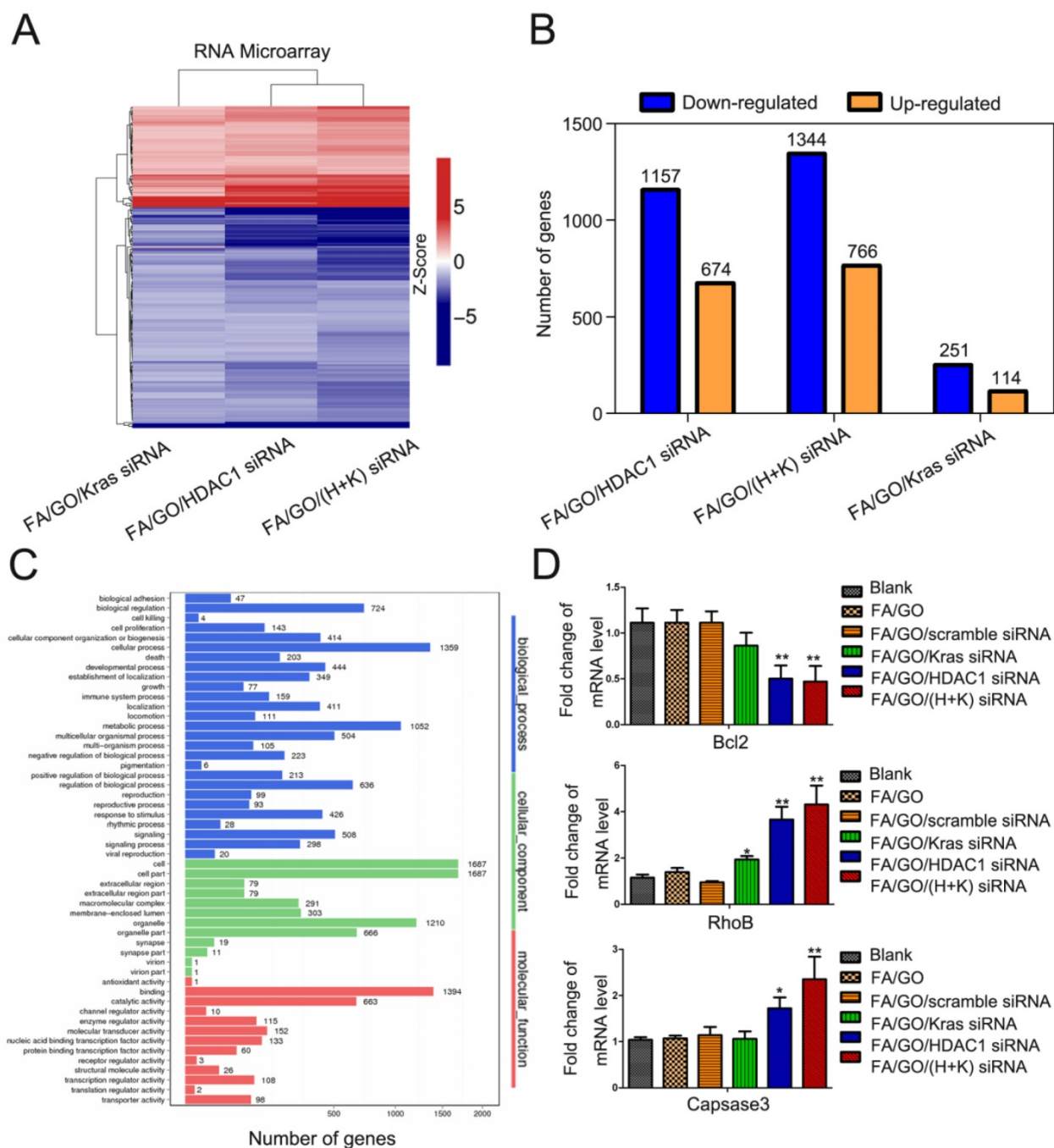
Figure 9. Transcriptome analysis of MIA PaCa-2 cells treated with different nanoformulations of PBS (blank), FA/GO/K-Ras siRNA, FA/GO/HDAC1 siRNA or FA/GO/(H+K) siRNA. (A) Heat-map of genes differentially expressed in RNA-microarray analysis performed on MIA PaCa-2 cells treated with FA/GO/K-Ras siRNA, FA/GO/HDAC1 siRNA or FA/GO/(H+K) siRNA compared to the PBS-treated control (blank). (B) Microarray analysis revealed a total of 1344 downregulated and 766 upregulated genes in MIA PaCa-2 cells with combined inactivation of HDAC1 and K-Ras (n = 3; fold change > 2.0; p < 0.05). (C) Gene ontology analysis revealed the different pathways involving these genes. (D) Downstream genes selected as candidates and confirmed by RT-PCR. Data are presented as means ± SEM of triplicate experiments. *, P < 0.05, **, P < 0.01 vs PBS (blank) and FA/GO.

Compared to mice treated with PBS or FA/GO/scramble siRNA nanoformulations, mice treated with FA/GO and NIR light or FA/GO/(HDAC1+K-Ras) siRNA showed 35% and 52% reduction of tumor volume, respectively. Moreover, the combination of FA/GO/(HDAC1+K-Ras) siRNA nanoformulations

and NIR light treatment provided the strongest effect in suppressing tumor growth *in vivo*, exhibiting a superior tumor growth inhibition rate of over 80% with minimal changes in the body weight of mice during the examination period. Furthermore, the mortality of mice during the survival study was assessed as shown in survival curves (Fig. S8C),

which suggested that the combination of FA/GO/(HDAC1+K-Ras) siRNA nanoformulations and NIR light treatment can be applied for long term cancer treatment. Intriguingly, the tumors diminished in 1/3 of the mice treated with FA/GO/(HDAC1+K-Ras) siRNA nanoformulations and NIR light after 60 days (Fig. S8D). It was worth mentioning that low levels of HDAC1 and K-Ras in FA/GO/siRNA nanoformulations-treated tumor tissues were detected by immunohistochemistry, which was consistent with the *in vitro* results (Fig. 5) and further demonstrated the gene knockdown efficiency of FA/GO/siRNA nanoformulations *in vivo* (Fig. S12).

GO-based nanoformulations show high biocompatibility and low toxicity *in vivo*

According to the results of the *in vitro* and *in vivo* experiments, FA-PEGylated GO-based nanosheets possess great potential as a novel siRNA delivery system that can be used for pancreatic cancer therapy. However, in order to develop successful applications for clinical treatments, it was essential to assess the *in vivo* use of nanomaterials to ensure that they were of low toxicity and could be eliminated from the body within a reasonable period of time. In the following studies, we designed a voluntary cage-wheel exercise assay and histological studies to assess the toxicity and biodistribution of GO nanoformulations in mice. In the voluntary cage-wheel exercise assay, BALB/c mice were randomly divided into two groups and subcutaneously injected with PBS or FA/GO (50 mg/kg). Over a period of 20 days after injection, the voluntary running cycles increased steadily with no significant differences between the two groups, indicating that treatment with FA/GO nanoformulations had no obvious effects on the motor learning ability of mice (Fig. S10). We then performed histological analyses to further evaluate the toxicity of FA/GO nanoformulations *in vivo* (Fig. S11). Major organs including the heart, liver, spleen, lung, kidneys and brain were harvested for hematoxylin and eosin (H&E) staining to observe histological changes 21 days after the injection of different FA/GO nanoformulations. Compared to PBS-treated mice, no signs of organ lesions were observed in mice treated with FA/GO nanoformulations. Moreover, the levels of HDAC1 and K-Ras were remarkably decreased by FA/GO/siRNA nanoformulations with NIR light, causing the change of apoptosis-related genes (Fig. S12). These *in vivo* toxicity assessments strongly indicate that FA/GO-based nanoformulations have low toxicity and could be a highly biocompatible nanocarrier for cancer therapy. Overall, the *in vivo* tumor inhibition assays clearly demonstrated that

HDAC1 and K-Ras play important roles in regulating pancreatic tumor growth. As such, the synergistic effects of the co-delivery of HDAC1 and K-Ras siRNA by GO combined with NIR light treatment may lead to a promising strategy for treating pancreatic adenocarcinoma *in vivo*.
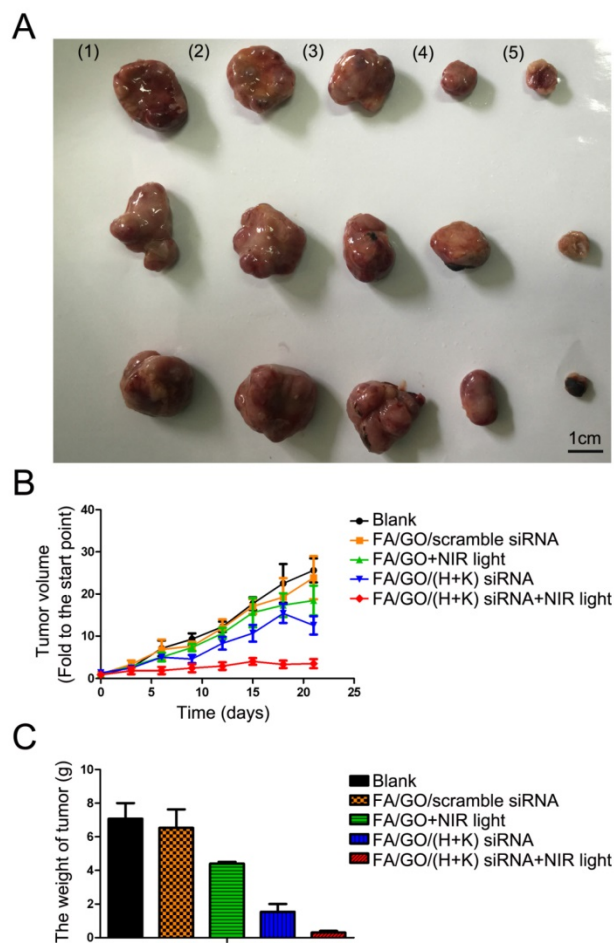

Figure 10. Antitumor activities of GO-based nanoformulations in a MIA PaCa-2 xenograft animal model. (A) Representative tumor tissue images of mice treated with (1) PBS, (2) FA/GO/scramble siRNA, (3) FA/GO with NIR light, (4) FA/GO/(H+K) siRNA or (5) FA/GO/(H+K) siRNA with NIR light. Mice treated with FA/GO/(H+K) siRNA with NIR light in the last group exhibited the smallest tumor size. (B) Relative changes in tumor volume over time and (C) tumor weights of mice treated with the same nanoformulations as in (A), respectively. Relative tumor volume was defined as $(V-V_0)/V_0$, where V and V_0 indicate the tumor volume on a particular day and day 0, respectively. Error bars represent SEMs for triplicate data. Mean tumor volumes were analyzed using one-way ANOVA. Values represent the means ± SEM, n=4-6 tumors.

Discussion

Pancreatic cancer is one of the most lethal cancers in the world characterized by extensive local tumor invasion and early systemic dissemination [55]. Due to the difficulty of early diagnosis and limited treatment options, the average life expectancy of patients after diagnosis is usually less than one year [56]. Chemotherapy and radiation therapy are the

preferred forms of treatment for patients with advanced pancreatic cancer. However, because the pancreas is difficult to palpate and there are no specific anti-pancreatic cancer drugs, these treatments only alleviate pancreatic cancer symptoms without long term cure [4]. Gene therapy is a novel approach in which nucleic acid polymers are delivered into a patient's cells as a drug to treat disease. Thanks to low toxicity and high gene knockdown efficiency, RNAi has attracted great attention as the most promising gene therapy strategy. However, the natural instability [42] and low uptake efficiency of siRNA *in vivo* [43] impede further applications of RNAi. In the last decade, several kinds of nanomaterials, such as AuNRs, quantum dots, silica nanoparticles and metal nanomaterials have been applied extensively as delivery systems and diagnostic agents for cancer diagnosis and treatment [57-59]. However, more detailed *in vivo* studies and a better understanding of the delivery mechanism will help the development of nanomedicine tremendously. Moreover, the potential toxicity and metabolism of these nanocarriers are critical issues that should be addressed before any *in vivo* use.

For the last decade, graphene has been extensively tested in numerous applications including electrochemistry, energy storage/conversion, tissue engineering and drug delivery. However, the toxicity of graphene remains an important issue to be resolved before it can be safely used for clinical research. Graphene oxide (GO) is a derivative of the one-atom thick graphene and the main precursor for the synthesis of graphene [60, 61]. Compared to graphene, graphene oxide has superior hydrophilicity and biocompatibility due to the availability of surface hydroxyl, carboxyl and epoxy groups which make it possible to modify the GO surface with desired biocompatible molecules or polymers to reduce the overall toxicity of GO. Furthermore, the strong absorption of GO in the near infrared region can induce photon-electron interactions to generate heat, which are widely used as photothermal reagents for the treatment of tumors and other diseases *in vivo*. The large specific surface area and the exceptional surface-to-volume ratio are incomparable advantages of graphene in drug or gene delivery applications in biomedicine [62, 63]. Many *in vitro* studies have demonstrated that graphene oxide has much lower toxicity than graphene. However, there have only been a few studies on the use of GO for *in vivo* applications so far [64, 65].

To date, functionalized GO has been applied for siRNA delivery extensively. However, there are no specific anti-pancreatic cancer nanodrugs that have utilized GO as an siRNA delivery nanocarrier *in vivo*

[19-21, 66]. This study is the first report of functionalized GO with FA/PEG to co-deliver HDAC1 and K-Ras siRNA for pancreatic cancer therapy *in vivo*, which showed better biocompatibility and stability in solution. Due to the high expression of folate receptor in MIA PaCa-2 cells, targeted delivery can be achieved by conjugation of FA with GO via receptor-mediated endocytosis [45, 46]. Previous reports suggested the synergetic inhibition of HDAC and KRAS as a more effective treatment of pancreatic ductal adenocarcinoma without toxicity to normal cells [7, 67], and the combination of HDAC1 siRNA with the MIA PaCa-2 cells-mutated K-Ras siRNA in our study can specifically inhibit the growth of MIA PaCa-2 cells with negligible side effects *in vitro* or *in vivo*. Moreover, according to previous reports, NIR irradiation could prompt the release of cargo molecules from GO [22, 23, 68, 69], which also explains the >80% inhibition of pancreatic cancer *in vivo* achieved with our GO nanomedicine treatment. As shown by fluorescence microscopy and flow cytometry analysis, both HDAC1 and K-Ras siRNA molecules were successfully delivered into MIA PaCa-2 cells by FA/GO-based nanocarriers with greater transfection efficiency than GO based nanocarriers or two commercial transfection reagents, because of FA induced targeted delivery. With the suppression of HDAC1 and K-Ras, cell proliferation and tumor growth were significantly inhibited. Transcriptome analysis further confirmed the inhibition mechanism of HDAC1 and K-Ras knockdown. According to these results, both HDAC1 and K-Ras play essential roles in regulating pancreatic cell proliferation, cell cycle progression and apoptosis, which is consistent with previous reports [39, 40, 70]. Because of the unique optical properties of GO nanosheets, the use of 808 nm NIR light enhances their anti-proliferative effects on pancreatic cancer cells. Our *in vivo* antitumor study shows that the synergistic effects of GO-based nanoformulations with NIR light reduced tumor volume growth by up to 80%. Moreover, 1/3 of the tumor-bearing mice were cured in our experiment by the synergistic effects of GO-siRNA nanoformulations with NIR light treatment. Also, the results of *in vivo* toxicity assessments show that GO has negligible toxicity. It is worth noting that tail vein injection of FA/GO nanoparticles resulted in quick death in mice, however, intraperitoneal injection had no side effects or associated mortality. This phenomenon emphasizes that suitable administration is crucial for the application of nanomedicines. In summary, this study reveals a novel and promising application of GO-based nanocarriers in cancer therapy combining gene therapy with photothermal effects. This may

further promote the biomedical applications of 2D nanomaterials for cancer theranostics and other diseases.

Supplementary Material

Supplementary figures and tables.
http://www.thno.org/v07p1133s1.pdf

Abbreviations

GO: Graphene oxide; siRNA: small interfering ribonucleic acid; NIR: near infrared radiation; PEG: Polyethylene Glycol; PAH: poly (allylamine hydrochloride); MTT: 3-(4,5-dimethylthiazol-2-yl)-2,5-diphenyltetrazolium bromides; Lipo: Lipofectamine 2000; Oligo: Oligofectamine; PBS: phosphate-buffered saline; FA: folic acid; HDAC1: Histone deacetylase 1; FACS: fluorescence activated cell sorting; FAM: Carboxyfluorescein; Cy3: Cyanine3.

Acknowledgements

Competing Interests

The authors have declared that no competing interest exists.

References

1. Cha CY, Shin SR, Annabi N, Dokmeci MR, Khademhosseini A. Carbon-Based Nanomaterials: Multifunctional Materials for Biomedical Engineering. Acs Nano. 2013; 7: 2891-7.
2. Schwendener RA. Liposomes in biology and medicine. Adv Exp Med Biol. 2007; 620: 117-28.
3. Tarn D, Ashley CE, Xue M, Carnes EC, Zink JI, Brinker CJ. Mesoporous silica nanoparticle nanocarriers: biofunctionality and biocompatibility. Acc Chem Res. 2013; 46: 792-801.
4. Yin F, Yang CB, Wang QQ, Zeng SW, Hu R, Lin GM, et al. A Light-Driven Therapy of Pancreatic Adenocarcinoma Using Gold Nanorods-Based Nanocarriers for Co-Delivery of Doxorubicin and siRNA. Theranostics. 2015; 5: 818-33.
5. Bekyarova E, Ni YC, Malarkey EB, Montana V, McWilliams JL, Haddon RC, et al. Applications of Carbon Nanotubes in Biotechnology and Biomedicine. J Biomed Nanotechnol. 2005; 1: 3-17.
6. Mazumder S, Dey R, Mitra MK, Mukherjee S, Das GC. Review: Biofunctionalized Quantum Dots in Biology and Medicine. J Nanomater. 2009.
7. Yin F, Lan RF, Zhang XM, Zhu LY, Chen FF, Xu ZS, et al. LSD1 Regulates Pluripotency of Embryonic Stem/Carcinoma Cells through Histone Deacetylase 1-Mediated Deacetylation of Histone H4 at Lysine 16. Mol Cell Biol. 2014; 34: 158-79.
8. Chen Y, Wang LZ, Shi JL. Two-dimensional non-carbonaceous materials-enabled efficient photothermal cancer therapy. Nano Today. 2016; 11: 292-308.
9. Novoselov KS, Geim AK, Morozov SV, Jiang D, Zhang Y, Dubonos SV, et al. Electric field effect in atomically thin carbon films. Science. 2004; 306: 666-9.
10. Avouris P, Xia FN. Graphene applications in electronics and photonics. Mrs Bull. 2012; 37: 1225-34.
11. Julkapli NM, Bagheri S. Graphene supported heterogeneous catalysts: An overview. Int J Hydrogen Energy. 2015; 40: 948-79.
12. Shao YY, Wang J, Wu H, Liu J, Aksay IA, Lin YH. Graphene Based Electrochemical Sensors and Biosensors: A Review. Electroanal. 2010; 22: 1027-36.
13. Raccichini R, Varzi A, Passerini S, Scrosati B. The role of graphene for electrochemical energy storage. Nat Mater. 2015; 14: 271-9.
14. Yang YQ, Asiri AM, Tang ZW, Du D, Lin YH. Graphene based materials for biomedical applications. Mater Today. 2013; 16: 365-73.
15. Yang LJ, Wang F, Han HE, Yang L, Zhang GS, Fan ZZ. Functionalized graphene oxide as a drug carrier for loading pirfenidone in treatment of subarachnoid hemorrhage. Colloids Surf B Biointerfaces. 2015; 129: 21-9.
16. Liu JQ, Cui L, Losic D. Graphene and graphene oxide as new nanocarriers for drug delivery applications. Acta Biomater. 2013; 9: 9243-57.
17. Bianco A. Graphene: Safe or Toxic? The Two Faces of the Medal. Angew Chem Int Edit. 2013; 52: 4986-97.
18. Feng LZ, Liu ZA. Graphene in biomedicine: opportunities and challenges. Nanomedicine-Uk. 2011; 6: 317-24.
19. Chen BA, Liu M, Zhang LM, Huang J, Yao JL, Zhang ZJ. Polyethylenimine-functionalized graphene oxide as an efficient gene delivery vector. J Mater Chem. 2011; 21: 7736-41.
20. Kim H, Namgung R, Singha K, Oh IK, Kim WJ. Graphene Oxide-Polyethylenimine Nanoconstruct as a Gene Delivery Vector and Bioimaging Tool. Bioconjug Chem. 2011; 22: 2558-67.
21. Feng LZ, Yang XZ, Shi XZ, Tan XF, Peng R, Wang J, et al. Polyethylene Glycol and Polyethylenimine Dual-Functionalized Nano-Graphene Oxide for Photothermally Enhanced Gene Delivery. Small. 2013; 9: 1989-97.
22. Li M, Yang XJ, Ren JS, Qu KG, Qu XG. Using Graphene Oxide High Near-Infrared Absorbance for Photothermal Treatment of Alzheimer's Disease. Adv Mater. 2012; 24: 1722-8.
23. Zhang W, Guo ZY, Huang DQ, Liu ZM, Guo X, Zhong HQ. Synergistic effect of chemo-photothermal therapy using PEGylated graphene oxide. Biomaterials. 2011; 32: 8555-61.
24. Chang YL, Yang ST, Liu JH, Dong E, Wang YW, Cao AN, et al. In vitro toxicity evaluation of graphene oxide on A549 cells. Toxicol Lett. 2011; 200: 201-10.
25. Sun XM, Liu Z, Welsher K, Robinson JT, Goodwin A, Zaric S, et al. Nano-Graphene Oxide for Cellular Imaging and Drug Delivery. Nano Res. 2008; 1: 203-12.
26. Wen HY, Dong CY, Dong HQ, Shen AJ, Xia WJ, Cai XJ, et al. Engineered Redox-Responsive PEG Detachment Mechanism in PEGylated Nano-Graphene Oxide for Intracellular Drug Delivery. Small. 2012; 8: 760-9.
27. Rosenberg SA, Aebersold P, Cornetta K, Kasid A, Morgan RA, Moen R, et al. Gene-Transfer into Humans - Immunotherapy of Patients with Advanced Melanoma, Using Tumor-Infiltrating Lymphocytes Modified by Retroviral Gene Transduction. New Engl J Med. 1990; 323: 570-8.
28. Yla-Herttuala S, Martin JF. Cardiovascular gene therapy. Lancet. 2000; 355: 213-22.
29. Kojima H, Fujimiya M, Matsumura K, Younan P, Imaeda H, Maeda M, et al. NeuroD-betacellulin gene therapy induces islet neogenesis in the liver and reverses diabetes in mice. Nat Med. 2003; 9: 596-603.
30. Hacein-Bey-Abina S, Hauer J, Lim A, Picard C, Wang GP, Berry CC, et al. Efficacy of Gene Therapy for X-Linked Severe Combined Immunodeficiency. New Engl J Med. 2010; 363: 355-64.
31. El-Aneed A. An overview of current delivery systems in cancer gene therapy. J Control Release. 2004; 94: 1-14.
32. Buckingham SD, Esmaeili B, Wood M, Sattelle DB. RNA interference: from model organisms towards therapy for neural and neuromuscular disorders. Hum Mol Genet. 2004; 13: R275-R88.
33. Aagaard L, Rossi JJ. RNAi therapeutics: Principles, prospects and challenges. Adv Drug Deliv Rev. 2007; 59: 75-86.
34. Lee JM, Yoon TJ, Cho YS. Recent Developments in Nanoparticle-Based siRNA Delivery for Cancer Therapy. Biomed Res Int. 2013.
35. Li SL, Liu ZH, Ji FT, Xiao ZJ, Wang MJ, Peng YJ, et al. Delivery of Quantum Dot-siRNA Nanoplexes in SK-N-SH Cells for BACE1 Gene Silencing and Intracellular Imaging. Mol Ther-Nucl Acids. 2012; 1.
36. Kuzmochka C, Abdou HS, Hache RJ, Atlas E. Inactivation of histone deacetylase 1 (HDAC1) but not HDAC2 is required for the glucocorticoid-dependent CCAAT/enhancer-binding protein alpha (C/EBPalpha) expression and preadipocyte differentiation. Endocrinol. 2014; 155: 4762-73.
37. Glozak MA, Seto E. Histone deacetylases and cancer. Oncogene. 2007; 26: 5420-32.
38. Xie HJ, Noh JH, Kim JK, Jung KH, Eun JW, Bae HJ, et al. HDAC1 Inactivation Induces Mitotic Defect and Caspase-Independent Autophagic Cell Death in Liver Cancer. Plos One. 2012; 7.
39. Wang SW, Yan-Neale Y, Fischer D, Zeremski M, Cai R, Zhu J, et al. Histone deacetylase 1 represses the small GTPase RhoB expression in human nonsmall lung carcinoma cell line. Oncogene. 2003; 22: 6204-13.
40. Delarue FL, Adnane J, Joshi B, Blaskovich MA, Wang DA, Hawker J, et al. Farnesyltransferase and geranylgeranyltransferase I inhibitors upregulate RhoB expression by HDAC1 dissociation, HAT association and histone acetylation of the RhoB promoter. Oncogene. 2007; 26: 633-40.
41. Lin GM, Hu R, Law WC, Chen CK, Wang YC, Chin HL, et al. Biodegradable Nanocapsules as siRNA Carriers for Mutant K-Ras Gene Silencing of Human Pancreatic Carcinoma Cells. Small. 2013; 9: 2757-63.

42. Whitehead KA, Langer R, Anderson DG. Knocking down barriers: advances in siRNA delivery. Nat Rev Drug Discov. 2009; 8: 129-38.

43. Shim MS, Kwon YJ. Efficient and targeted delivery of siRNA in vivo. Febs J. 2010; 277: 4814-27.

44. Fleming JB, Shen GL, Holloway SE, Davis M, Brekken RA. Molecular consequences of silencing mutant K-ras in pancreatic cancer cells: Justification for K-ras-directed therapy. Mol Cancer Res. 2005; 3: 413-23.

45. Sudimack J, Lee RJ. Targeted drug delivery via the folate receptor. Adv Drug Deliv Rev. 2000; 41: 147-62.

46. Hu R, Law WC, Lin GM, Ye L, Liu JW, Liu J, et al. PEGylated Phospholipid Micelle-Encapsulated Near-Infrared PbS Quantum Dots for in vitro and in vivo Bioimaging. Theranostics. 2012; 2: 723-33.

47. Cheng L, Yang K, Li YG, Chen JH, Wang C, Shao MW, et al. Facile Preparation of Multifunctional Upconversion Nanoprobes for Multimodal Imaging and Dual-Targeted Photothermal Therapy. Angew Chem Int Edit. 2011; 50: 7385-90.

48. Loryuenyong V, Totepvimarn K, Eimburanapravat P, Boonchompoo W, Buasri A. Preparation and Characterization of Reduced Graphene Oxide Sheets via Water-Based Exfoliation and Reduction Methods. Adv Mater Sci Eng. 2013.

49. Liang YY, Li YG, Wang HL, Zhou JG, Wang J, Regier T, et al. Co3O4 nanocrystals on graphene as a synergistic catalyst for oxygen reduction reaction. Nat Mater. 2011; 10: 780-6.

50. Chen JQ, Wang XP, Chen TS. Facile and green reduction of covalently PEGylated nanographene oxide via a 'water-only' route for high-efficiency photothermal therapy. Nanoscale Res Lett. 2014; 9.

51. Matias R, Ribeiro PRS, Sarraguca MC, Lopes JA. A UV spectrophotometric method for the determination of folic acid in pharmaceutical tablets and dissolution tests. Anal Methods-Uk. 2014; 6: 3065-71.

52. Ropero S, Esteller M. The role of histone deacetylases (HDACs) in human cancer. Mol Oncol. 2007; 1: 19-25.

53. Jasim DA, Menard-Moyon C, Begin D, Bianco A, Kostarelos K. Tissue distribution and urinary excretion of intravenously administered chemically functionalized graphene oxide sheets. Chem Sci. 2015; 6: 3952-64.

54. Yang K, Gong H, Shi XZ, Wan JM, Zhang YJ, Liu Z. In vivo biodistribution and toxicology of functionalized nano-graphene oxide in mice after oral and intraperitoneal administration. Biomaterials. 2013; 34: 2787-95.

55. Keleg S, Buchler P, Ludwig R, Buchler MW, Friess H. Invasion and metastasis in pancreatic cancer. Mol cancer. 2003; 2: 14.

56. Vincent A, Herman J, Schulick R, Hruban RH, Goggins M. Pancreatic cancer. Lancet. 2011; 378: 607-20.

57. Ray PC, Yu HT, Fu PP. Toxicity and Environmental Risks of Nanomaterials: Challenges and Future Needs. J Environ Sci Heal C. 2009; 27: 1-35.

58. Yildirimer L, Thanh NT, Loizidou M, Seifalian AM. Toxicology and clinical potential of nanoparticles. Nano Today. 2011; 6: 585-607.

59. Pan Y, Wang L, Kang SG, Lu Y, Yang Z, Huynh T, et al. Gd-Metallofullerenol Nanomaterial Suppresses Pancreatic Cancer Metastasis by Inhibiting the Interaction of Histone Deacetylase 1 and Metastasis-Associated Protein 1. Acs Nano. 2015; 9: 6826-36.

60. Hansora DP, Shimpi NG, Mishra S. Graphite to Graphene via Graphene Oxide: An Overview on Synthesis, Properties, and Applications. Jom-Us. 2015; 67: 2855-68.

61. Zhu YW, Murali S, Cai WW, Li XS, Suk JW, Potts JR, et al. Graphene and Graphene Oxide: Synthesis, Properties, and Applications. Adv Mater. 2010; 22: 3906-24.

62. Chung C, Kim YK, Shin D, Ryoo SR, Hong BH, Min DH. Biomedical Applications of Graphene and Graphene Oxide. Acc Chem Res. 2013; 46: 2211-24.

63. Yang K, Feng LZ, Shi XZ, Liu Z. Nano-graphene in biomedicine: theranostic applications. Chem Soc Rev. 2013; 42: 530-47.

64. Zhao XB, Liu P. Biocompatible graphene oxide as a folate receptor-targeting drug delivery system for the controlled release of anti-cancer drugs. Rsc Adv. 2014; 4: 24232-9.

65. Yang XY, Niu GL, Cao XF, Wen YK, Xiang R, Duan HQ, et al. The preparation of functionalized graphene oxide for targeted intracellular delivery of siRNA. J Mater Chem. 2012; 22: 6649-54.

66. Yin D, Li Y, Lin H, Guo BF, Du YW, Li X, et al. Functional graphene oxide as a plasmid-based Stat3 siRNA carrier inhibits mouse malignant melanoma growth in vivo. Nanotechnology. 2013; 24.

67. Ischenko I, Petrenko O, Hayman MJ. A MEK/PI3K/HDAC inhibitor combination therapy for KRAS mutant pancreatic cancer cells. Oncotarget. 2015; 6: 15814-27.

68. Bai J, Liu YW, Jiang XE. Multifunctional PEG-GO/CuS nanocomposites for near-infrared chemo-photothermal therapy. Biomaterials. 2014; 35: 5805-13.

69. Shi JJ, Wang L, Zhang J, Ma R, Gao J, Liu Y, et al. A tumor-targeting near-infrared laser-triggered drug delivery system based on GO@Ag nanoparticles for chemo-photothermal therapy and X-ray imaging. Biomaterials. 2014; 35: 5847-61.

70. Jiang K, Sun JZ, Cheng J, Djeu JY, Wei S, Sebti S. Akt mediates ras downregulation of RhoB, a suppressor of transformation, invasion, and metastasis. Mol Cell Biol. 2004; 24: 5565-76.